Optical Engineering

SPIEDigitalLibrary.org/oe

Grating lobes analysis based on blazed grating theory for liquid crystal optical-phased array

Jian Chen
Guolong Cui
Lingjiang Kong
Feng Xiao
Xin Liu
Xiaoguang Zhang

SPIE

Grating lobes analysis based on blazed grating theory for liquid crystal optical-phased array

Jian Chen
Guolong Cui
Lingjiang Kong
Feng Xiao
University of Electronic Science and Technology of China
School of Electronic Engineering
Chengdu 610054, China
E-mail: lingjiang.kong@gmail.com

Xin Liu
Xiaoguang Zhang
Science and Technology on Electro-Optical Information Security Control Laboratory
Sanhe 065201, China

Abstract. The grating lobes of the liquid crystal optical-phased array (LCOPA) based on blazed grating theory is studied. Using the Fraunhofer propagation principle, the analytical expressions of the far-field intensity distribution are derived. Subsequently, we can obtain both the locations and the intensities of the grating lobes. The derived analytical functions that provide an insight into single-slit diffraction and multislit interference effect on the grating lobes are discussed. Utilizing the conventional microwave-phased array technique, the intensities of the grating lobes and the main lobe are almost the same. Different from this, the derived analytical functions demonstrate that the intensities of the grating lobes are less than that of the main lobe. The computer simulations and experiments show that the proposed method can correctly estimate the locations and the intensities of the grating lobes for a LCOPA simultaneously. [DOI: 10.1117/1.OE.52.9.097102]

Subject terms: grating lobes; liquid crystal optical-phased array; blazed grating theory; microwave-phased array.

Paper 130953 received Jun. 28, 2013; revised manuscript received Aug. 11, 2013; accepted for publication Aug. 14, 2013; published online Sep. 10, 2013.

1 Introduction

Liquid crystal optical-phased array (LCOPA) can realize a nonmechanical beam steering by applying the required voltage profile to the phase elements. Compared with the mechanical beam directing systems, it has remarkable advantages, such as low-power consumption, programmability, precise stabilization, low weight, random-access pointing, insensitivity to acceleration, and high-pointing accuracy. Thus, LCOPA has the potential applications in missile interceptors, satellite communications, and laser radar.[1–3] In the past decades, LCOPA has received considerable attentions, and the performance has been improved significantly. For example, nonmechanical beam steering over a 45×45-deg field of regard had been demonstrated in 2004, and the diffraction efficiency is 15% to 20%.[4] By utilizing the lithographic process technique, LCOPA can be integrated on a liquid crystal waveplate. Hence, the pitch between adjacent phase elements (center to center) can be made smaller and smaller, and the pixel pitch for LCOPA had been decreased to 1.6 μm by Boulder Nonlinear Systems.[5]

The presence of grating lobes in LCOPA will disperse the energy of the output beam and degrade the diffraction efficiency. Unfortunately, the grating lobes are unavoidable for LCOPA due to the limitation of the state-of-art and the wavelength of radiation. Even the pixel pitch mentioned above is not small enough to avoid the grating lobes for LCOPA in the visible or near-IR region, because the required pixel pitch is less than half a micron according to the conventional microwave-phased array theory.[6,7] By exploiting the conventional microwave-phased array technique, the grating lobes for optical-phased array are studied.[8] This technique can only accurately predict the locations of the grating lobes. However, the intensities of these grating lobes obtained by this technique are the same as that of the main lobe, which is not consistent with the experimental results in practice.

In this article, we address the problem of correctly predicting both the locations and the intensities of the grating lobes simultaneously. Specifically, we first introduce the blazed grating models of LCOPA. In fact, when the designed phase profile is applied to LCOPA to steer the incident beam to the desired direction, the LCOPA can be seen as a blazed grating,[9] which can be classified into the period blazed grating and nonperiod blazed grating.[10,11] The period one is similar to the binary optical elements and can steer the incident beam to some discrete angles. The nonperiod one can realize the uniform, continuous beam scanning in the field-of-view of LCOPA.[11] Then, we analyze the far-field intensity distribution after the incident beam transmitting through LCOPA, using the Fraunhofer propagation principle.[12,13] We obtain the analytical functions of the far-field intensity distributions as well as the locations and the intensities of the grating lobes for both the models. Finally, we evaluate the performance of the derived functions via computer simulations and experiments.

2 Grating Lobes Analysis for LCOPA

This section is devoted to formulating mathematically the far-field intensity distributions for the period blazed grating and nonperiod blazed grating models of LCOPA, i.e., getting the analytical expressions for each case.

2.1 *Period Blazed Grating Model for LCOPA*

We consider one-dimensional LCOPA with N phase elements, as shown in Fig. 1. Assume that the width of the phase element is small enough, so that each element can be seen as a narrow slit, and the diffraction theory of light can be used to calculate the far-field light distribution.

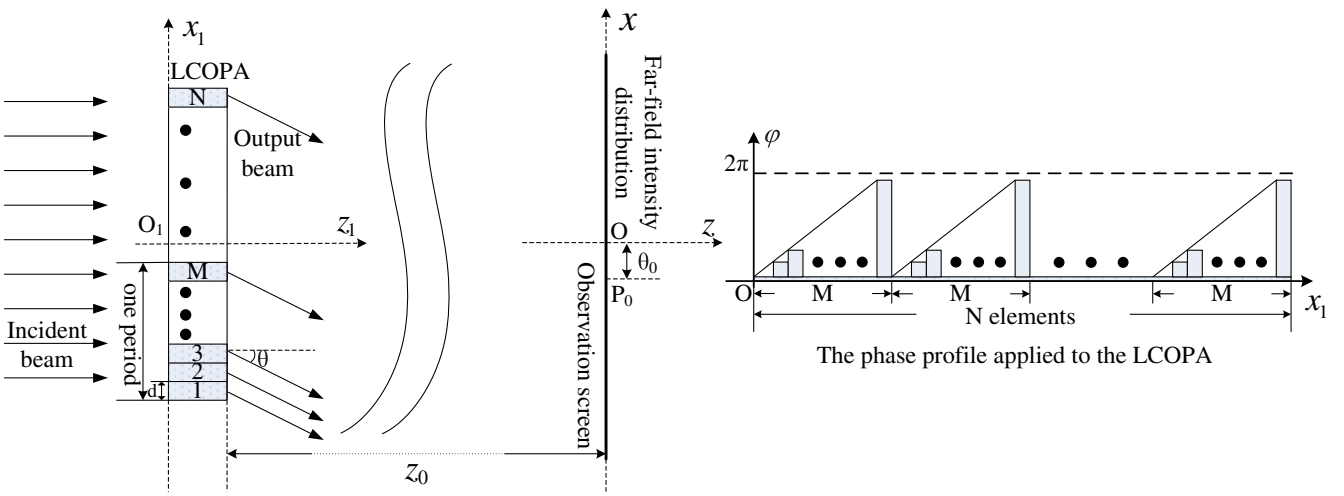

Fig. 1 Schematic of the period blazed grating model for liquid crystal optical-phased array (LCOPA).

For the case of one-dimension, the Fraunhofer diffraction function can be written as[12]

$$E(P) = \frac{\exp(jkz_0)}{j\lambda z_0}\exp\left(j\frac{kx^2}{2z_0}\right)\int \bar{E}(x_1)\exp\left(-j\frac{k}{z_0}xx_1\right)\mathrm{d}x_1, \tag{1}$$

where $\bar{E}(x_1)$ is the electric field component of the output beam, $E(P)$ is the electric field distribution on the observation screen (i.e., far-field light distribution), $k = 2\pi/\lambda$ denotes the wave vector, λ is the wavelength of the incident beam, z_0 is the distance between the LCOPA and the observation screen, x_1 is the horizontal ordinate of Cartesian coordinate in the plane of LCOPA, and x is the horizontal ordinate of Cartesian coordinate in the plane of the observation screen. The thickness of the LCOPA is in the orders of magnitude of micron, so it can be neglected.

Assume that the phase elements in the LCOPA are independent, and the incident beam is steered to the deflection angle θ_0 with respect to the normal direction of LCOPA, namely the point P_0 in Fig. 1. Then, the phase retardation difference $\Delta\varphi_\mathrm{p}$ between adjacent elements in one period can be written as

$$\Delta\varphi_\mathrm{p} = 2\pi/M, \tag{2}$$

where M denotes the period corresponding to the deflection angle θ_0. Herein, we set the first phase element to the M_th phase element as a period, and then the phase retardation of each element in the period can be denoted as

$$\varphi_m = m\Delta\varphi_\mathrm{p} \quad m = 0, 1, 2, \cdots, M-1. \tag{3}$$

Suppose the incident beam is plane light with zero initial phase and unit amplitude, the electric field component $E_\mathrm{p}(x_1)$ of the output beam, after the incident beam transmitting through the phase elements in the aforementioned period, can be given by

$$E_\mathrm{p}(x_1) = \sum_{m=0}^{M-1} e^{-j\varphi_m}\mathrm{rect}\left(\frac{x_1 - md - d/2}{d}\right), \tag{4}$$

where d denotes the width of the phase element. The electric field component $E(x_1)$ of the output beam, after the incident beam transmitting through the entire LCOPA, can be obtained by extending Eq. (4) periodically. For an integer N/M, the extension function can be expressed as

$$f(x_1) = \sum_{n=0}^{N/M-1}\delta(x_1 - nMd), \tag{5}$$

where $\delta(\cdot)$ is delta function, which is defined as

$$\delta(x) = \begin{cases} 0 & x \neq 0 \\ \infty & x = 0 \end{cases} \quad \text{and} \quad \int_{-\infty}^{\infty}\delta(x)\mathrm{d}x = 1. \tag{6}$$

Substituting Eq. (3) into Eq. (4) and using Eq. (5), we can obtain

$$E(x_1) = f(x_1) \otimes E_\mathrm{p}(x_1) = \sum_{n=0}^{N/M-1}\delta(x_1 - nMd) \otimes \sum_{m=0}^{M-1} e^{-jm\Delta\varphi_\mathrm{p}}\mathrm{rect}\left(\frac{x_1 - md - d/2}{d}\right), \tag{7}$$

where $\otimes$ is the convolution operator, namely

$$f(t) \otimes g(t) = \int_{-\infty}^{\infty} f(\tau)g(t-\tau)\mathrm{d}\tau. \tag{8}$$

Combining Eq. (7) with Eq. (1) and ignoring the constant term, the far-field light distribution $E(P)$ on the observation screen can be derived as

$$E(P) = E_1 \cdot E_2 \cdot E_3$$

$$E_1 = \exp\left[-j(N-1)\frac{\pi M d \sin\theta}{\lambda}\right]\frac{\sin\left(\frac{\pi N d \sin\theta}{\lambda}\right)}{\sin\left(\frac{\pi M d \sin\theta}{\lambda}\right)}$$

$$E_2 = \exp\left(-j\frac{\pi d \sin\theta}{\lambda}\right)\frac{\sin\frac{\pi d \sin\theta}{\lambda}}{\frac{\pi \sin\theta}{\lambda}}$$

$$E_3 = \exp\left[-j\frac{M-1}{2}\left(\Delta\varphi_p + \frac{2\pi d \sin\theta}{\lambda}\right)\right] \times \frac{\sin\left[\frac{M}{2}\left(\Delta\varphi_p + \frac{2\pi d \sin\theta}{\lambda}\right)\right]}{\sin\left[\frac{1}{2}\left(\Delta\varphi_p + \frac{2\pi d \sin\theta}{\lambda}\right)\right]}, \quad (9)$$

where E_1 is the interaction between periods, one period can be seen as a combining element that is similar to the single physical phase element; E_2 is single-slit diffraction; and E_3 is multislit interference in one period. Based on Eq. (9), the far-field intensity distribution $I(P)$ is

$$I(P) = |E(P)|^2 = A_1 \cdot A_2 \cdot A_3$$

$$A_1 = |E_1|^2 = \left|\frac{\sin\left(\frac{\pi N d \sin\theta}{\lambda}\right)}{\sin\left(\frac{\pi M d \sin\theta}{\lambda}\right)}\right|^2$$

$$A_2 = |E_2|^2 = \left|\frac{\sin\frac{\pi d \sin\theta}{\lambda}}{\frac{\pi \sin\theta}{\lambda}}\right|^2$$

$$A_3 = |E_3|^2 = \left|\frac{\sin\left[\frac{M}{2}\left(\Delta\varphi_p + \frac{2\pi d \sin\theta}{\lambda}\right)\right]}{\sin\left[\frac{1}{2}\left(\Delta\varphi_p + \frac{2\pi d \sin\theta}{\lambda}\right)\right]}\right|^2. \quad (10)$$

Based on Eq. (10), when the denominator of A_3 is equal to zero, namely θ_m meeting Eq. (11), the grating lobes come into being.

$$\Delta\varphi_p + \frac{2\pi d \sin\theta_m}{\lambda} = 2\,m\pi \qquad m = \pm 1, \pm 2, \cdots. \quad (11)$$

To avoid the grating lobes, all angle θ should meet the following inequality:

$$\left|\Delta\varphi_p + \frac{2\pi d \sin\theta}{\lambda}\right| < 2\pi. \quad (12)$$

Using Eq. (2), we get the solution of Eq. (12) in the following form:

$$d < \lambda\left(1 - \frac{1}{M}\right) \le \frac{\lambda}{2}. \quad (13)$$

The laser steered by LCOPA is usually a visible or a near-IR laser, whose wavelength is in the orders of magnitude of micron. As is mentioned in the Sec. 1, the width of the phase element cannot be decreased to less than 1 μm to date; thus, the grating lobes are inevitable for LCOPA. Using Eqs. (2) and (11), we can obtain the locations of the grating lobes θ_m

$$\theta_m = \arcsin\left[\frac{\lambda}{d}\left(m - \frac{1}{M}\right)\right] \qquad m = \pm 1, \pm 2, \cdots. \quad (14)$$

Substituting Eq. (14) into Eq. (10), one can get the intensity of the m_{th} grating lobe $I(m)$

$$I(m) = N^2 \cdot \left|\frac{d \sin\left[\pi\left(m - \frac{1}{M}\right)\right]}{\pi\left(m - \frac{1}{M}\right)}\right|^2. \quad (15)$$

It is remarked that the locations of the grating lobes are mainly determined by A_3 in Eq. (10), namely the multislit interference in one period; suppressed by A_2 in Eq. (10), i.e., the single-slit diffraction, the amplitudes of the grating lobes are less than that of the main lobe.

2.2 *Nonperiod Blazed Grating Model for LCOPA*

The nonperiod blazed grating model for LCOPA is shown in Fig. 2. Assume that the phase elements in the LCOPA are independent, and the incident beam is plane light with zero initial phase and unit amplitude.

When the incident beam is steered to the direction θ_0 with respect to the normal direction of LCOPA (i.e., the point P_0 in Fig. 2), the phase retardation difference $\Delta\varphi_{np}$ between adjacent elements can be written as

$$\Delta\varphi_{np} = -\frac{2\pi d \sin\theta_0}{\lambda}. \quad (16)$$

The electric field component $E_{np}(x_1)$ of the output beam, after the incident beam is transmitted through the entire LCOPA, can be expressed as

$$E_{np}(x_1) = \sum_{m=0}^{N-1} e^{-jm\Delta\varphi_{np}} \operatorname{rect}\left(\frac{x_1 - md - d/2}{d}\right). \quad (17)$$

Substituting Eq. (17) into Eq. (1) and using Eq. (16), we get the far-field light distribution $E_{np}(P)$ on the observation screen (ignoring the constant term)

$$E_{np}(P) = E_{np1} \cdot E_{np2}$$

$$E_{np1} = \exp\left(-j\frac{\pi d \sin\theta}{\lambda}\right)\frac{\sin\left(\frac{\pi d \sin\theta}{\lambda}\right)}{\frac{\pi \sin\theta}{\lambda}}$$

$$E_{np2} = \exp\left[-j(N-1)\frac{\pi d(\sin\theta - \sin\theta_0)}{\lambda}\right]\frac{\sin\left[\frac{\pi N d(\sin\theta - \sin\theta_0)}{\lambda}\right]}{\sin\left[\frac{\pi d(\sin\theta - \sin\theta_0)}{\lambda}\right]}, \quad (18)$$

where E_{np1} is single-slit diffraction and E_{np2} is multislit interference. From Eq. (18), the far-field intensity distribution $I_{np}(P)$ can be derived as

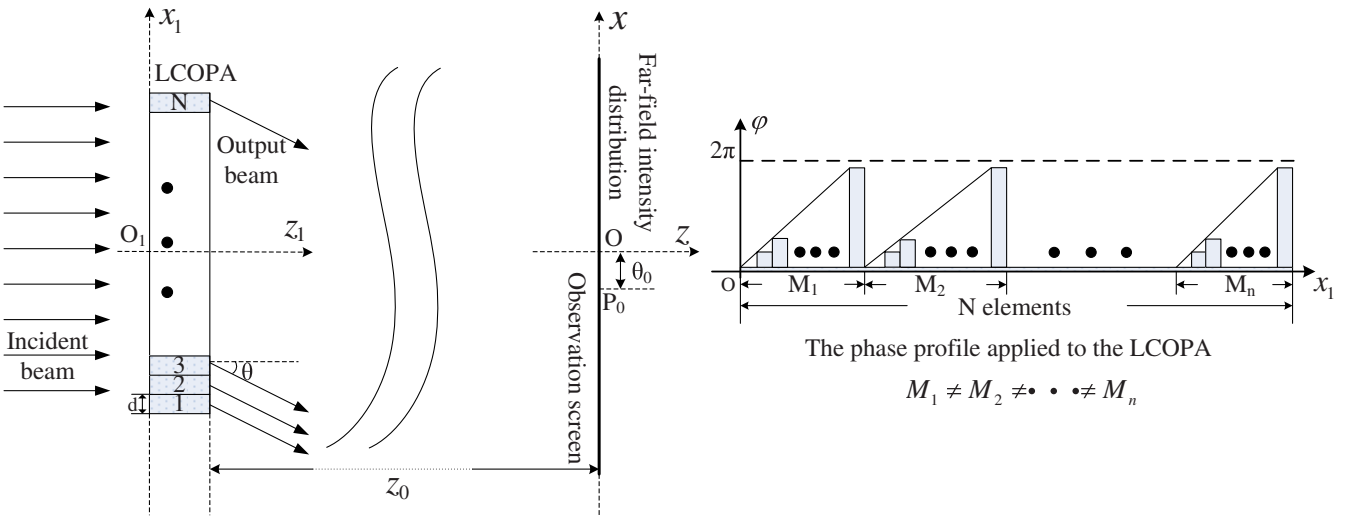

Fig. 2 Schematic of the nonperiod blazed grating model for LCOPA.

$$I_{np}(P) = |E_{np}(P)|^2 = A_{np1} \cdot A_{np2}$$

$$A_{np1} = |E_{np1}|^2 = \left| \frac{\sin \frac{\pi d \sin\theta}{\lambda}}{\frac{\pi \sin\theta}{\lambda}} \right|^2$$

$$A_{np2} = |E_{np2}|^2 = \left| \frac{\sin\left[\frac{\pi N d(\sin\theta - \sin\theta_0)}{\lambda}\right]}{\sin\left[\frac{\pi d(\sin\theta - \sin\theta_0)}{\lambda}\right]} \right|^2. \quad (19)$$

Based on Eq. (19), we can get the same conclusion as that in Sec. 2.1, i.e., the grating lobes are inevitable for LCOPA at present. From Eq. (19), the locations of the grating lobes θ_n are determined by A_{np2} (the multislit interference), which is given by

$$\theta_n = \arcsin\left(\frac{n\lambda}{d} + \sin\theta_0\right) \qquad n = \pm 1, \pm 2, \pm 3, \cdots. \quad (20)$$

Substituting Eq. (20) into Eq. (19), one can get the intensity of the n_{th} grating lobe $I_{np}(n)$.

$$I_{np}(n) = N^2 \cdot \left| \frac{\sin\left[\frac{\pi d}{\lambda}\left(\frac{n\lambda}{d} + \sin\theta_0\right)\right]}{\frac{\pi}{\lambda}\left(\frac{n\lambda}{d} + \sin\theta_0\right)} \right|^2. \quad (21)$$

Equation (19) indicates that the intensities of grating lobes are less than that of the main lobe, which is identical to the results obtained by Eq. (10).

3 Computer Simulations

In this section, we evaluate the performance of the derived solutions Eqs. (10) and (19) in the previous section via computer simulations for both the period and nonperiod blazed grating model. Note that the negative sign of an angle denotes steering the incident beam to the left, and the positive sign of an angle denotes steering the incident beam to the right in the simulations.

3.1 *Period Blazed Grating for LCOPA*

We first consider the period blazed grating for a 1920-element LCOPA, whose phase element width is 5 μm. The incident beam is plane light with zero initial phase and unit amplitude, whose wavelength is 0.6328 μm. Suppose that the phase period is 16, and the incident beam is steered to the right side of the normal direction of the LCOPA along the propagating direction of incident beam.

The normalized far-field intensity distribution of the simulation is shown in Fig. 3. From the figure, we can see that −2nd, −1st, 1st, and 2nd orders are the grating lobes and 0th order is the main lobe. When the angle range is limited to [−20 deg, 20 deg], the normalized far-field intensity distribution calculated by Eq. (10) is shown in Fig. 4.

Inspection on the normalized far-field intensity distribution in Figs. 3 and 4 reveals that the intensities of the grating lobes are less than that of the main lobe for the period blazed grating of LCOPA. To compare the simulation results with the theoretical results, the values of the peak points in Figs. 3 and 4 are shown in Table 1.

The angle error is calculated by

$$\theta_{\text{error}} = \frac{|\theta_{\text{Sim}} - \theta_{\text{The}}|}{|\theta_{\text{The}}|}, \quad (22)$$

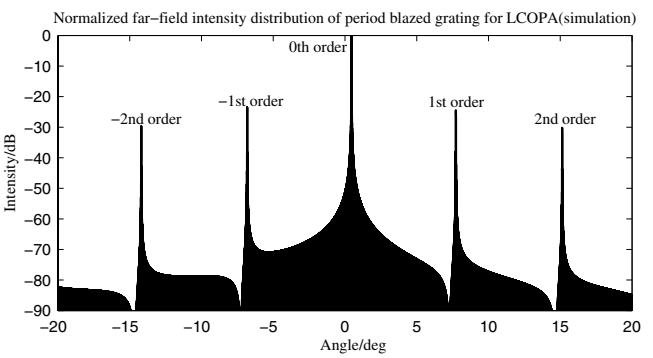

Fig. 3 Results of period blazed grating simulation for LCOPA.

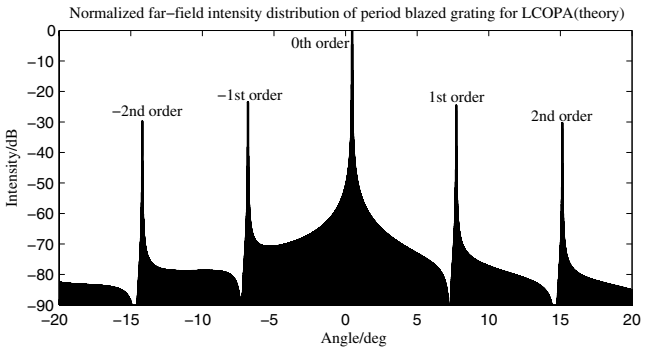

Fig. 4 Far-field intensity distribution calculated by Eq. (10).

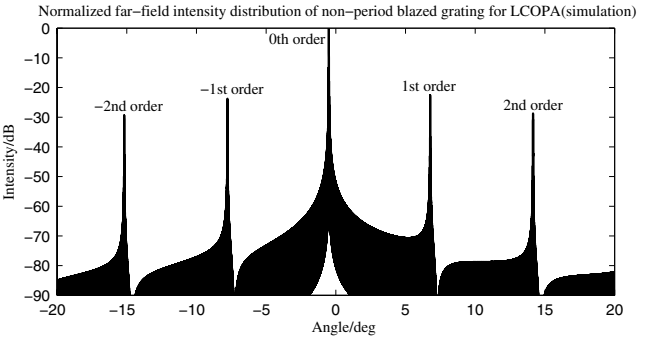

Fig. 5 Results of nonperiod blazed grating simulation for LCOPA.

where θ_{Sim} is the simulation values of the locations of the main lobe and grating lobes and θ_{The} is the corresponding theoretical values. The intensity error is defined as

$$I_{\mathrm{error}} = \frac{|I_{\mathrm{Sim}} - I_{\mathrm{The}}|}{|I_{\mathrm{The}}|}, \tag{23}$$

where I_{Sim} is the simulation values of the intensities of the grating lobes and I_{The} is the corresponding theoretical values.

Some observations are now in order from Table 1. First, the locations of the grating lobes of theoretical solution Eq. (14) are identical to these of simulations. Second, the intensity errors of the grating lobes between simulations and the theoretical solution Eq. (15) are less than 0.5%. Consequently, it can be concluded that the simulation results are in an excellent agreement with the theoretical results for period blazed grating of LCOPA.

3.2 *Nonperiod Blazed Grating for LCOPA*

In this section, we consider the nonperiod blazed grating for a 1920-element LCOPA, whose phase element width is also 5 μm. The incident beam is plane light with zero initial phase and unit amplitude operating at $\lambda = 0.6328$ μm. Assume that the incident beam is steered to the left of 0.5 deg with respect to the normal direction of the LCOPA along the propagating direction of incident beam.

Figure 5 depicts the normalized far-field intensity distribution of the simulation. When the angle range is limited to [−20 deg, 20 deg], the normalized far-field intensity distribution calculated by Eq. (19) is shown in Fig. 6. It can be seen from Figs. 5 and 6 that the intensities of the grating lobes are less than that of the main lobe for the nonperiod blazed grating of LCOPA.

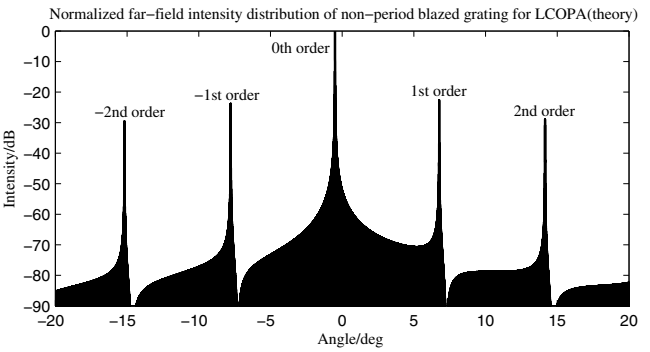

Fig. 6 Far-field intensity distribution calculated by Eq. (19).

To compare the simulation results with the theoretical results, the values of the peak points in Figs. 5 and 6 are shown in Table 2. The angle and intensity errors in Table 2 are calculated by Eqs. (22) and (23), respectively. Some observations are now in order from Table 2. First, the locations of the grating lobes of the theoretical solution in Eq. (20) are identical to simulations. Second, the intensity errors of the grating lobes between simulations and the theoretical solution in Eq. (21) are less than 0.6%. Hence, it can be remarked that the simulation results agree excellently with the theoretical results for nonperiod blazed grating of LCOPA.

Table 1 Values of the peak points in Figs. 3 and 4.

Order number		−2nd	−1st	0th	1st	2nd
Angle (deg)	Simulation value	−14.19	−6.81	0.45	7.73	15.13
	Theory value	−14.19	−6.81	0.45	7.73	15.13
Angle error (%)		0.00	0.00	0.00	0.00	0.00
Intensity (dB)	Simulation value	−29.69	−23.49	0.00	−24.57	−30.22
	Theory value	−29.83	−23.52	0.00	−24.61	−30.37
Intensity error (%)		0.47	0.13	0.00	0.16	0.49

Table 2 Values of the peak points in Figs. 5 and 6.

Order number		−2nd	−1st	0th	1st	2nd
Angle (deg)	Simulation value	−15.18	−7.78	−0.50	6.77	14.15
	Theory value	−15.18	−7.78	−0.50	6.77	14.15
Angle error (%)		0.00	0.00	0.00	0.00	0.00
Intensity (dB)	Simulation value	−29.39	−23.77	0.00	−22.58	−28.81
	Theory value	−29.55	−23.81	0.00	−22.61	−28.95
Intensity error (%)		0.54	0.17	0.00	0.13	0.48

4 Experimental Verifications

In this section, we assess the proposed solutions in Eqs. (10) and (19) via experimental data. In Fig. 7, we provide the schematic of experimental setup, which is composed of (1) laser operating at $\lambda = 0.6328$ μm; (2) diaphragm; (3) 1920-element LCOPA with the element width of 5 μm; (4) controller, applying the voltage code to the LCOPA; (5) PC, generating the voltage code; (6) camera, photographing the diffraction pattern on the observation screen; and (7) observation screen with a distance of 118 cm from the LCOPA. This experimental setup is employed in both period blazed grating and nonperiod blazed grating experiment of LCOPA.

4.1 *Period Blazed Grating for LCOPA*

We first consider the experiment of period blazed grating based on LCOPA to study the grating lobes. The phase period is 16, which is the same as that in Sec. 3.1. The incident beam was steered to the right of the normal direction of LCOPA along the propagating direction of incident beam.

Figure 8 is the far-field intensity distribution observed on the observation screen for the period blazed grating experiment. As shown in Fig. 8, we can observe the main lobe (0th order) and the grating lobes (−1st and 1st orders) obviously. However, the grating lobes (−2nd and 2nd orders) are indistinct. The reason is the power of the laser used in the experiment is about 3 mW, so that the grating lobes (−2nd and 2nd orders) are so weak that the camera can hardly image them. In addition, there are other bright spots between the main lobe and the grating lobes in Fig. 8. The fringing-field effect between adjacent elements in LCOPA is considered to be the main factor that give rise to these unwanted spots, since the fringing-field effect broadens the designed phase profile applied to the LCOPA.[14,15] Phase valley and flyback region are other reasons leading to this problem, because they

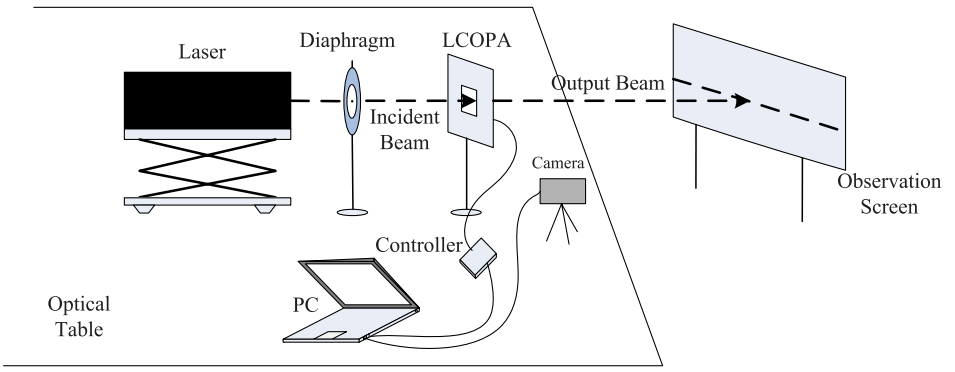

Fig. 7 Schematic of experimental setup.

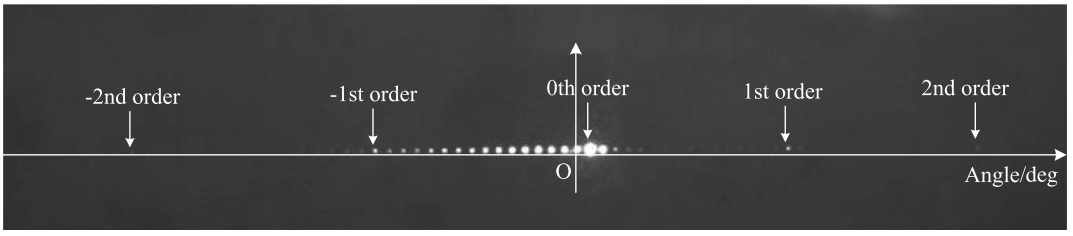

Fig. 8 Experimental results of period blazed grating for LCOPA.

Table 3 Values of the main lobe and the grating lobes in Fig. 8.

Order number	−2nd	−1st	0th	1st	2nd
Experiment value of angle (deg)	−14.15	−6.81	0.46	7.79	15.33
Angle error (%)	0.28	0.00	2.22	0.78	1.32
Experiment value of intensity (dB)	−30.77	−24.19	0.00	−24.77	−28.47
Intensity error (%)	3.15	2.85	0.00	0.65	6.26

distort the designed phase profile.[16,17] The values (including locations and intensities) of the main lobe and grating lobes pointed out in Fig. 8 are shown in Table 3 and are compared with the corresponding theoretical values. The angle error is calculated by

$$\theta_{\text{error}} = \frac{|\theta_{\text{Exp}} - \theta_{\text{The}}|}{|\theta_{\text{The}}|}, \tag{24}$$

where θ_{Exp} is the experimental values of the locations of the main lobe and the grating lobes and θ_{The} is the corresponding theoretical values, which can be obtained from Table 1. The intensity error is defined as

$$I_{\text{error}} = \frac{|I_{\text{Exp}} - I_{\text{The}}|}{|I_{\text{The}}|}, \tag{25}$$

where I_{Exp} is the experimental values of intensities of the grating lobes and I_{The} is the corresponding theoretical values, which can be obtained from Table 1.

Some analyses of Table 3 are in order. First, the angle errors of the locations of the main lobe and the grating lobes between experiment and theoretical solution in Eq. (14) are very small, less than 2.3%. The influencing factors, including measurement error, voltage quantization,[18] surface deformation of LCOPA,[19] nonuniformity of lead resistance,[20] etc., cause the angle error. Second, the intensity errors of the grating lobes between experiment and theoretical solution in Eq. (15) are acceptable, less than 6.3%, caused mainly by the fringing-field effect, flyback region, phase valley, and measurement error. Inspection on the experimental values of intensities in Table 3 reveals that the intensities of the grating lobes are less than that of the main lobe, which confirms the conclusion obtained by Eq. (10). Herein, it can be concluded that the experimental results are in a good agreement with the theoretical results for period blazed grating of LCOPA.

4.2 *Nonperiod Blazed Grating for LCOPA*

In this section, we consider the experiment of nonperiod blazed grating based on LCOPA. The incident beam is steered to the left of 0.5 deg with respect to the normal direction of the LCOPA along the propagating direction of the incident beam, which is same as in Sec. 3.2.

Figure 9 displays the far-field intensity distribution seen on the observation screen for the nonperiod blazed grating experiment. Inspection on Fig. 9 reveals that the main lobe (0th order) and the grating lobes (−1st and 1st orders)

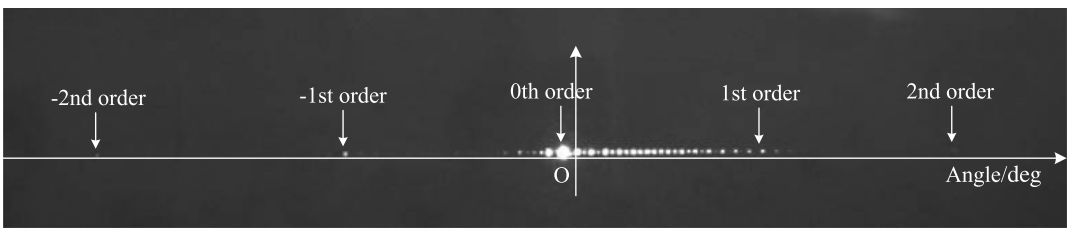

Fig. 9 Experimental results of nonperiod blazed grating for LCOPA.

Table 4 Values of the main lobe and the grating lobes in Fig. 9.

Order number	−2nd	−1st	0th	1st	2nd
Experiment value of angle (deg)	−15.06	−7.77	−0.51	6.81	14.31
Angle error (%)	0.79	0.13	2.00	0.59	1.13
Experiment value of intensity (dB)	−30.61	−25.14	0.00	−23.68	−28.77
Intensity error (%)	3.59	5.59	0.00	4.73	0.62

are evident. Because of the low power (3 mW) of the laser used in the experiment, the grating lobes (−2nd and 2nd orders) are indistinct. There are also some undesired bright spots in Fig. 9. As described in Sec. 4.1, the fringing-field effect and other factors cause these undesired spots. The values (including locations and intensities) of the main lobe and the grating lobes pointed out in Fig. 9 are shown in Table 4 and are compared with the corresponding theoretical values.

The angle and intensity errors in Table 4 are calculated by Eqs. (24) and (25), respectively, and the corresponding theoretical values can be obtained from Table 2. Some analyses of Table 4 are in order. First, the angle errors of the locations of the main lobe and the grating lobes between experimental results and theoretical solutions in Eq. (20) are also very small, less than 2%. The factors causing the angle error are the same as those mentioned in subsection 4.1. Second, the intensity errors of the grating lobes between experimental results and theoretical solutions in Eq. (21) are acceptable, less than 5.6%. The fringing-field effect, measurement error, and other factors cause the intensity error. Based on the experimental values of the intensities in Table 4, one can see the intensities of the grating lobes are less than that of the main lobe, which agrees with the results achieved by Eq. (19). Thus, it can be remarked that the experimental results agree well with the theoretical results for nonperiod blazed grating of LCOPA.

5 Conclusions

In this article, we have addressed the grating lobes of LCOPA based on the blazed grating theory.

1. Two blazed grating models for LCOPA are introduced, i.e., period blazed grating and nonperiod blazed grating models.
2. The analytical expressions of the far-field intensity distribution functions, which are used to exploit both the locations and the intensities of the grating lobes, are derived according to the Fraunhofer propagation principle for each case. The derived analytical functions, i.e., Eqs. (10) and (19), provide an insight for single-slit diffraction and multislit interference effects on the grating lobes. From Eqs. (10) and (19), it can be seen that the intensities of the grating lobes are less than that of the main lobe, due to the suppression of the single-slit diffraction.
3. Computer simulations and experimental verifications are carried out to evaluate the derived analytical expressions. Both of them are compared with the theoretical results. The good agreement obtained in these comparisons demonstrates that the analysis of grating lobes based on the blazed grating theory is reasonable and is more suitable to be employed for LCOPA than the conventional microwave technique.

The possible future research track might concern mathematically modeling the unwanted bright spots between the main lobe and the grating lobes. Many factors such as fringing-field effect, phase valley, and flyback region give rise to these spots.[14–17] It might be of interest to study effective methods to suppress the grating lobes to a lower level, so as to focus the energy of the output beam to the main lobe.

Acknowledgments

This work was sponsored by National Natural Science Foundation of China (61178068 and 61201276) and Defense Industrial Technology Development Program (B1120110006).

References

1. P. F. McManamon et al., "Optical phased array technology," *Proc. IEEE* **84**(2), 268–298 (1996).
2. P. F. McManamon and E. A. Watson, "Optical beam steering using phased array technology," *Proc. SPIE* **3131**, 90–98 (1997).
3. X. Z. Wang, Q. Li, and Q. Wang, "Progress and analysis of the liquid crystal phased array technology in ladar," in *Proc. RCSLPLT/ASOMT 2010*, pp. 273–276 (2010).
4. P. F. McManamon, "An overview of optical phased array technology and status," *Proc. SPIE* **5947**, 59470I (2005).
5. A. Linnenberger and S. Serati, "Advances in optical phased array technology," *Proc. SPIE* **6304**, 63040T (2007).
6. Z. S. He and W. Xia, *Modern Digital Signal Processing and Application*, Tsinghua University Press, Beijing (2010).
7. G. Y. Zhang, *Principles of Phased Array Radar*, National Defense Industry Press, Beijing (2009).
8. S. Yin et al., "Ultra-fast speed, low grating lobe optical beam scanning using unequally spaced phased array technique," *Opt. Commun.* **270**(1), 41–46 (2007).
9. R. M. Matic, "Blazed phase liquid crystal beam steering," *Proc. SPIE* **2120**, 194–205 (1994).
10. P. F. McManamon and E. A. Watson, "Design of optical phased array beam steering with limited dispersion," in *Proc. IEEE*, Vol. 3, pp. 1583–1591 (2001).
11. L. J. Kong et al., "A beam steering approach of liquid crystal phased array based on non-periodic blazed grating," *Acta Opt. Sin.* **31**(1), 0123001 (2011).
12. J. W. Goodman, *Introduction to Fourier Optics*, Publishing House of Electronics Industry, Beijing (2011).
13. D. Y. Yu and H. Y. Tan, *Engineering Optics*, China Machine Press, Beijing (2011).
14. E. Uzi, A. Boris, and B. T. Eldad, "Studies of fringing field effects in liquid crystal beam-steering devices," *Proc. SPIE* **5936**, 59360P (2005).
15. X. H. Wang et al., "Modeling and design of an optimized liquid-crystal optical phased array," *J. Appl. Phys.* **98**(7), 073101 (2005).
16. L. Xu et al., "Effect of phase valley on diffraction efficiency of liquid crystal optical phased array," *Proc. SPIE* **7133**, 71333L (2009).
17. L. Xu and Z. Q. Huang, "Quantitative analysis on flyback region problem of 1D transmissive liquid crystal optical phased array devices," *Proc. SPIE* **7658**, 76580N (2010).
18. L. J. Kong et al., "Research on scanning accuracy of liquid crystal phased array component of laser radar," *Chin. J. Lasers* **36**(5), 1080–1085 (2009).
19. B. Wang et al., "2-D liquid crystal optical phased array," in *Proc. IEEE*, Vol. 2, pp. 905–912 (2004).
20. Z. H. Lin, L. J. Kong, and X. B. Yang, "The influence factors analysis on the steering performances of liquid crystal optical phased array," in *Proc. IEEE* Vol. 2, pp. 1131–1134 (2011).

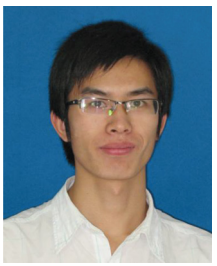

Jian Chen received his BS degree from Southwest University of Science and Technology, Mianyang, Sichuan, China in 2011. Now, he is a PhD student for signal and information processing at University of Electronic Science and Technology of China (UESTC). His research interests are mainly in lidar based on liquid crystal optical-phased array.

Guolong Cui received his BS, MS, and PhD degrees from University of Electronic Science and Technology of China (UESTC) in 2005, 2008, and 2012, respectively. He is currently a postdoc in Stevens Institute of Technology, Hoboken, New Jersey. From January 2011 to April 2011, he was a visiting student researcher with University of Naples Federico II, Naples, Italy. His research interests lies in the field of statistical signal processing with emphasis on radar detection and liquid crystal optical-phased array.

Lingjiang Kong received his BS, MS, and PhD degrees from University of Electronic Science and Technology of China (UESTC) in 1997, 2000, and 2003, respectively. From September 2009 to March 2010, he was a visiting researcher with the University of Florida, USA. He is currently a professor in the School of Electronic Engineering, UESTC. His research interests are mainly in new type radar system, such as MIMO radar, through the wall radar, statistical signal processing, and liquid crystal optical-phased array.

Feng Xiao received his BS in optical engineering from University of Electronic Science and Technology of China (2010). He is now a PHD candidate in school of Electronic Engineering, University of Electronic Science and Technology of China. His major is signal and information processing, and his research interests are mainly about optical phased array technology and radar system.

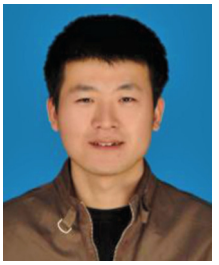

Xin Liu received his MS degree from Dalian University of Technology, Dalian, China in 2008. He is currently a senior engineer at Science and Technology on Electro-Optical Information Security Control Laboratory, Sanhe, China. His current research interests include laser physics and electro-optical information security.

Xiaoguang Zhang received his master's degree from Jilin University and PhD degree from University of Science and Technology Beijing. He is interested in optical-electro functional materials and optical-electro system design.